

Temporal response of a random medium from speckle intensity frequency correlations

Mark A. Webster, Kevin J. Webb, and Andrew M. Weiner

*School of Electrical and Computer Engineering, Purdue University, 1285 Electrical Engineering Building,
465 Northern Avenue, West Lafayette, Indiana 47907-1285*

Junying Xu and Hui Cao

Department of Physics and Astronomy, Materials Research Center, Northwestern University, Evanston, Illinois 60208

Received December 9, 2002; revised manuscript received June 2, 2003; accepted July 1, 2003

We reconstruct the temporal response of a random medium by using speckle intensity frequency correlations. When the scattered field from a random medium is described by circular complex Gaussian statistics, we show that third-order correlations permit retrieval of the Fourier phase of the temporal response with bispectral techniques. Our experimental results for random media samples in the diffusion regime are in excellent agreement with the intensity temporal response measured directly with an ultrafast pulse laser and a streak camera. Our speckle correlation measurements also demonstrate sensitivity to inhomogeneous samples, highlighting the potential application for imaging within a scattering medium. © 2003 Optical Society of America

OCIS codes: 030.6140, 290.4210, 290.1990, 290.7050, 100.5070.

1. INTRODUCTION

The study of wave propagation in random media is important for atmospheric and other environmental sensing applications.¹ Also, of recent importance is the study of near-IR light within biological tissue for imaging and spectroscopy,² especially for tumor detection. Biological tissue belongs to an important class of random media where the transport of light is well described by the diffusion approximation. A random medium in the diffusion regime has a mean free path much greater than the wavelength (also called the weak-scattering limit), with a sample size much larger than the mean free path, such that a large amount of multiple scattering is present.³

Coherent light propagating through a random medium will produce fluctuations in the measured intensity due to interference of the multiply scattered partial waves, which is the well-known speckle phenomenon.⁴ The statistical properties of the speckle field carry information about the scattering properties of the random medium and the coherence properties of the illumination. For example, Parry⁵ investigated the relationship between surface roughness and the coherence length of a laser source, Bellini *et al.*⁶ studied the effect of finite laser coherence for light propagating through a dynamic random medium, and Genack⁷ measured the autocorrelation of intensity fluctuations from light propagating through a random medium as the laser frequency was tuned, i.e., the second-order intensity correlation in frequency was measured. In recent studies, Thompson *et al.*^{8,9} determined the dependence of the speckle contrast as a function of the diffusive random medium thickness for a finite coherence source, and McKinney *et al.*¹⁰ measured the speckle contrast as a function of a variable source coherence, synthe-

sized by scanning the center frequency of a laser diode rapidly relative to the detector integration time.

The intensity temporal response of a random medium provides important information about the scattering properties, such as the mean free path of a random medium, and can be used as the basis for imaging in diffusive media such as biological tissue.^{11–15} We recently introduced the use of third-order intensity correlations in frequency as a means to determine the temporal response.¹⁶ In this paper, we provide details of this approach and supporting streak camera data.

Our key result is the experimental demonstration of the use of third-order intensity frequency correlations of speckle patterns to obtain the temporal response. Third-order correlations can provide the Fourier phase of the temporal response, which is not available from the commonly used second-order correlations. It has been demonstrated that the temporal response of a random medium can be obtained from second-order intensity correlations only when *a priori* information is used, such as in assuming a form for the temporal response, based on a diffusion model for example, and fitting unknown parameters.^{10,17} No such assumptions are necessary with third-order correlations. For our work, any multiple-scattering random medium can be studied, provided that the fields obey circular Gaussian statistics.

Third-order correlations have been investigated in the past for several different applications. An extension to the intensity interferometer of Hanbury Brown and Twiss¹⁸ was proposed for measuring the optical power spectrum of a light source by Gamo.^{19,20} Lohmann *et al.*²¹ used third-order correlations in a speckle masking technique for astronomical imaging. The recovery of the

intensity pulse shape from a short pulse laser by using third-order correlations was proposed by Blount and Klauder,²² who also established that third-order correlations are sufficient to fully characterize the intensity pulse shape.

For random media in the strong-scattering limit (where the mean free path is comparable with the wavelength), there have been many studies on intensity correlations investigating the contributions of short-range, long-range, and infinite-range terms to the measured correlation.^{3,23–26} For optical experiments in the weak-scattering limit and the diffusion regime, which we investigate here, the long-range and infinite-range correlation effects are negligible²⁶ and ignored for this study.

In Section 2 of this paper, a model for the scattered field from a random medium is developed, and the conditions for Gaussian statistics to apply are established. The frequency correlation behavior is presented, the intensity temporal response is derived, and the diffusion approximation is discussed. Section 3 discusses the bispectrum and its application to reconstructing the temporal response with third-order intensity correlation measurements. Section 4 details the experimental results for both the speckle intensity correlations and the direct measurement of the intensity temporal response with an ultrafast pulse laser and a streak camera.

2. THEORY

A. Scattered Field from a Random Medium

When a monochromatic field illuminates a random medium, the total field at a particular point after traversing the medium can be expressed as the superposition of many scattered partial waves. Each of these partial waves has a random magnitude and a random phase, relative to the incident wave, thus allowing the total field to be described by a random phasor sum. This random phasor sum model is the foundation for the statistical description of speckle discussed by Goodman,⁴ and it was developed for light reflected from (or transmitted through) a rough surface but applies equally to a random medium consisting of many scatterers.

Using the random phasor sum model, we obtain a convenient and general expression for the scattered field from a time-invariant random medium. We assume a scalar model for the scattered electric field, which physically means that we consider only a single linear polarization. However, it should be possible to extend this approach to a generalized vectorial model.

At some specified source location on the random medium, the applied monochromatic electric field of frequency ν is

$$e_{\text{in}}(t) = E_i \exp(j2\pi\nu t) + \text{c.c.}, \quad (1)$$

where E_i is the complex amplitude and c.c. represents the complex conjugate. Then, at some specified detector location, the resultant linearly polarized electric field is represented as

$$e_{\text{out}}(t) = E_o(\nu)\exp(j2\pi\nu t) + \text{c.c.}, \quad (2)$$

where the output electric field complex amplitude $E_o(\nu)$ is a random variable dependent upon the frequency of the

applied field. The statistical properties of the random medium can be studied by using the statistics of $E_o(\nu)$. The random phasor sum model represents $E_o(\nu)$ as²⁷

$$E_o(\nu) = \frac{1}{\sqrt{N}} \sum_{k=1}^N A_k \exp[-j\phi_k(\nu)], \quad (3)$$

where A_k is the random magnitude and $\phi_k(\nu)$ is the random phase of the k th elementary partial wave. The number of elementary partial waves is given by N , which is assumed to be large so that the limit $N \rightarrow \infty$ can be used. The random magnitudes A_k are modeled independent of frequency, because we assume that the scattering cross sections of the scatterers do not vary with small changes in frequency and can therefore be considered frequency independent. The random phase, on the other hand, is very sensitive to small changes in frequency. Each random phase $\phi_k(\nu)$ is modeled as an accumulated phase from traversing the k th path whose random “time of flight” is t_k , resulting in

$$\phi_k(\nu) = 2\pi\nu t_k. \quad (4)$$

We therefore assume elastic scattering.

For the random phasor sum model to be practical for gaining insight into the response of a random medium, several assumptions need to be made about the statistical properties of the scattered partial waves. As did Goodman,⁴ we assume the following: (i) The random magnitudes A_k are statistically independent and identically distributed, (ii) the random phases $\phi_k(\nu)$ are statistically independent and uniformly distributed over the interval $-\pi$ to π when taken mod 2π , and (iii) the random magnitude A_k and the random phase $\phi_k(\nu)$ of each elementary partial wave are statistically independent. These assumptions are equivalent to specifying that the elementary partial waves, represented by the magnitude and phase terms in the random phasor sum model in Eq. (3), are all statistically independent.

In Eq. (4), we relate the random phases to the random (independent and identically distributed) times of flight t_k , which in general will not be uniformly distributed but have a probability density function that we denote by $p(t)$. As long as the width of $p(t)$ is broad compared with $1/\nu$, the random phases will be approximately uniform when taken mod 2π , supporting assumption (ii). For our study, the optical frequency ν is approximately $3.5 \times 10^{14} \text{ s}^{-1}$ (a wavelength of 850 nm), and, for the samples studied, $p(t)$ has a width of the order of 10^{-10} s or greater.

B. Statistics of the Scattered Field

Under assumptions (i)–(iii) listed in Subsection 2.A, the output field $E_o(\nu)$ from a random medium, measured at a single frequency ν and modeled by the random phasor sum in Eq. (3), has first-order statistics that are zero-mean circular complex Gaussian. In this case, the speckle field statistics are also called “fully developed.”⁴ When we write $E_o(\nu) = x + jy$, the joint probability density function for the real and imaginary parts is

$$p_{xy}(x, y) = \frac{1}{2\pi\sigma^2} \exp\left(-\frac{1}{2} \frac{x^2 + y^2}{\sigma^2}\right), \quad (5)$$

where

$$\sigma^2 = \frac{1}{N} \sum_{k=1}^N \frac{\langle A_k^2 \rangle}{2}. \quad (6)$$

The brackets $\langle \cdot \rangle$ represent the ensemble average over all possible scatterer configurations of the random medium. By assuming that the random magnitudes A_k are identically distributed, we further simplify the expression in Eq. (6) to $\sigma^2 = \langle A^2 \rangle / 2$. The output intensity from a random medium is given by $I(\nu) = |E_o(\nu)|^2$, whose ensemble average is calculated from Eq. (5) to give $\langle I(\nu) \rangle = 2\sigma^2$. This result shows that assuming that the random magnitudes are frequency independent (for small frequency variations), along with assumptions (i)–(iii), implies that the ensemble average output intensity is also frequency independent:

$$\langle I \rangle = \langle A^2 \rangle. \quad (7)$$

We show that the temporal response of a random medium can be obtained by determining the correlations between the speckle intensity patterns measured at two or more different frequencies. This development requires knowledge of the higher-order field statistics. As shown in Appendix A, under assumptions (i)–(iii), the statistics for the set of scattered fields $E_o(\nu_1), E_o(\nu_2), \dots, E_o(\nu_M)$ measured at different frequencies are jointly zero-mean circular complex Gaussian. The output field random vector measured at M discrete frequencies is

$$\mathbf{z} = \begin{pmatrix} E_o(\nu_1) \\ E_o(\nu_2) \\ \vdots \\ E_o(\nu_M) \end{pmatrix}. \quad (8)$$

The joint probability density function for the random vector \mathbf{z} is, from Appendix A,

$$p_z(\mathbf{z}) = \frac{1}{\pi^M |\mathbf{C}_z|} \exp(-\mathbf{z}^H \mathbf{C}_z^{-1} \mathbf{z}), \quad (9)$$

where \mathbf{z}^H is the Hermitian transpose of \mathbf{z} and \mathbf{C}_z is the complex covariance matrix whose (i, j) th element is given by $[\mathbf{C}_z]_{i,j} = \langle E_o(\nu_i) E_o^*(\nu_j) \rangle$. Because \mathbf{z} is circular complex Gaussian, as shown in Appendix A, the Gaussian moment theorem of Reed²⁸ can be used to express high-order moments as a sum of products of second-order moments, which are the elements of \mathbf{C}_z .

C. Frequency Correlations of the Scattered Field

The scattered partial waves in a random medium have a distribution for the times of flight that we denote by the probability density function $p(t)$. Let the spread in the time-of-flight distribution be Δt , where, for instance, $\Delta t = \sqrt{\langle t^2 \rangle - \langle t \rangle^2}$. From the uncertainty relation, $E_o(\nu)$ will become uncorrelated with $E_o(\nu + \Delta\nu)$ when the change in frequency $\Delta\nu$ satisfies the condition $\Delta\nu \Delta t \sim 1$. Genack^{17,29} gives the second-order correlation between two fields at different frequencies:

$$\langle E_o(\nu + \Delta\nu) E_o^*(\nu) \rangle = \langle I \rangle P(\Delta\nu), \quad (10)$$

where $P(\Delta\nu)$ is the Fourier transform of $p(t)$, given by

$$P(\Delta\nu) = \int_{-\infty}^{\infty} dt p(t) \exp(-j2\pi\Delta\nu t). \quad (11)$$

A derivation of this result, based on assumptions (i)–(iii) in Subsection 2.A, is given in Appendix B. The samples studied in this paper have a spread in the time-of-flight distribution in the range $\Delta t \sim 0.1$ – 1.0 ns. Hence the frequency bandwidth after which the fields in Eq. (10) become uncorrelated will be approximately $\Delta\nu \sim 1$ – 10 GHz.

In practice, it is usually quite difficult to measure the field second-order correlation of Eq. (10) directly at optical frequencies for light scattered by a random medium. On the other hand, it is convenient to measure the intensity second-order correlation $\langle I(\nu + \Delta\nu) I(\nu) \rangle$. This correlation is fourth order in field, and since the field statistics are circular complex Gaussian, the Gaussian moment theorem²⁸ can be applied with Eq. (10) to give

$$\langle I(\nu + \Delta\nu) I(\nu) \rangle = \langle I \rangle^2 + \langle I \rangle^2 |P(\Delta\nu)|^2. \quad (12)$$

The second-order intensity correlation contains information only about the Fourier magnitude of $p(t)$. Since the Fourier phase information is lost, it is not possible to reconstruct $p(t)$ from measurements of second-order intensity correlations without using *a priori* information, which was the approach investigated in previous studies.^{10,17}

It was recently shown¹⁶ that third-order intensity correlations do contain sufficient information about the Fourier phase of $p(t)$ to allow reconstruction of $p(t)$ from intensity-based measurements without recourse to an assumed model for $p(t)$. The third-order intensity correlation, which is a sixth-order field correlation, can again be evaluated by the Gaussian moment theorem²⁸ and the use of Eq. (10) to give

$$\begin{aligned} \langle I(\nu) I(\nu + \Delta\nu_1) I(\nu + \Delta\nu_2) \rangle &= \langle I \rangle^3 + \langle I \rangle^3 |P(\Delta\nu_1)|^2 + \langle I \rangle^3 |P(\Delta\nu_2)|^2 \\ &+ \langle I \rangle^3 |P(\Delta\nu_1 + \Delta\nu_2)|^2 + 2\langle I \rangle^3 \text{Re}\{P(\Delta\nu_1) \\ &\times P(\Delta\nu_2) P^*(\Delta\nu_1 + \Delta\nu_2)\}. \end{aligned} \quad (13)$$

It is mathematically convenient to define a normalized intensity $\tilde{I} = (I - \langle I \rangle) / \langle I \rangle$, in which case the second-order and third-order correlations of the normalized intensity respectively become

$$\langle \tilde{I}(\nu + \Delta\nu) \tilde{I}(\nu) \rangle = |P(\Delta\nu)|^2, \quad (14)$$

$$\begin{aligned} \langle \tilde{I}(\nu) \tilde{I}(\nu + \Delta\nu_1) \tilde{I}(\nu + \Delta\nu_1 + \Delta\nu_2) \rangle &= 2 \text{Re}\{P(\Delta\nu_1) P(\Delta\nu_2) \\ &\times P^*(\Delta\nu_1 + \Delta\nu_2)\}. \end{aligned} \quad (15)$$

Identifying that the normalized intensity third-order correlation in Eq. (15) is equal to the real component of the bispectrum³⁰ of $p(t)$ is a key observation.¹⁶ This result permits a bispectral technique^{30,31} to be used for reconstructing $p(t)$, and this is described in Section 3.

D. Intensity Temporal Response

We show that the normalized ensemble average intensity temporal response is equal to the time-of-flight distribu-

tion $p(t)$. In Subsection 4.D, we present measured streak camera data in excellent agreement with the results obtained from speckle correlations.

The electric field of an ultrafast pulse applied to the random medium is given by $a_{\text{in}}(t)$, and the output field is given by $a_{\text{out}}(t)$. Both these real signals have an optical center frequency ν_0 and are written as

$$a_{\text{in}}(t) = u(t)\exp(j2\pi\nu_0 t) + \text{c.c.}, \quad (16)$$

$$a_{\text{out}}(t) = v(t)\exp(j2\pi\nu_0 t) + \text{c.c.}, \quad (17)$$

where $u(t)$ and $v(t)$ are the pulse complex amplitude envelope functions of the input and output signals, respectively. The function $v(t)$ is the complex stochastic output field envelope from a random medium in response to the deterministic input complex envelope $u(t)$. The output intensity measured by a photodetector will have an ensemble average value

$$\langle I(t) \rangle = \langle |v(t)|^2 \rangle. \quad (18)$$

Remaining consistent with linear system theory,³² if the response of a linear system to the input signal $\exp(j2\pi\nu t)$ is the output signal $H(\nu)\exp(j2\pi\nu t)$, then $H(\nu)$ is the transfer function of the linear system. Referring to Eqs. (1) and (2), we see that the transfer function of a random medium is the output field: $H(\nu) = E_o(\nu)/E_i$. Therefore the second-order correlation of the random medium transfer function can be written, by using Eq. (10), as

$$\langle H(\nu + \Delta\nu)H^*(\nu) \rangle = \langle |H(\nu)|^2 \rangle P(\Delta\nu), \quad (19)$$

where the quantity $\langle |H(\nu)|^2 \rangle = \langle I \rangle / |E_i|^2$ is a constant.

Denoting the Fourier transforms of $v(t)$ as $V(\nu)$ and of $u(t)$ as $U(\nu)$, we can use the relation $V(\nu) = U(\nu)H(\nu + \nu_0)$ to express $v(t)$ as

$$v(t) = \int_{-\infty}^{\infty} d\nu U(\nu)H(\nu + \nu_0)\exp(j2\pi\nu t). \quad (20)$$

Substituting Eq. (20) into Eq. (18) gives the ensemble average intensity

$$\begin{aligned} \langle I(t) \rangle = & \left\langle \int_{-\infty}^{\infty} d\nu' U(\nu')H(\nu' + \nu_0)\exp(j2\pi\nu' t) \right. \\ & \left. \times \int_{-\infty}^{\infty} d\nu'' U^*(\nu'')H^*(\nu'' + \nu_0)\exp(-j2\pi\nu'' t) \right\rangle. \end{aligned} \quad (21)$$

After we interchange the order of integration, perform the ensemble averaging, and make the variable substitutions $\Delta\nu = \nu' - \nu''$ and $\nu = \nu''$, Eq. (21) becomes

$$\begin{aligned} \langle I(t) \rangle = & \int_{-\infty}^{\infty} d\nu \int_{-\infty}^{\infty} d\Delta\nu \langle H(\nu + \nu_0 + \Delta\nu) \\ & \times H^*(\nu + \nu_0) \rangle U(\nu + \Delta\nu)U^*(\nu)\exp(j2\pi\Delta\nu t). \end{aligned} \quad (22)$$

With the use of Eq. (19), $\langle H(\nu + \nu_0 + \Delta\nu)H^*(\nu + \nu_0) \rangle = \langle |H(\nu + \nu_0)|^2 \rangle P(\Delta\nu)$. Also, if the bandwidth of the input pulse is broad compared with the frequency range over which $P(\Delta\nu)$ is nonzero, then $U(\nu + \Delta\nu) \approx U(\nu)$. This approximation can be interpreted as having the tem-

poral width of the input pulse much smaller than the temporal features in the time-of-flight distribution $p(t)$. This requirement is necessary if we wish to accurately probe the structure of $p(t)$. Under these conditions, Eq. (22) simplifies to

$$\langle I(t) \rangle = \int_{-\infty}^{\infty} d\nu \langle |V(\nu)|^2 \rangle \int_{-\infty}^{\infty} d\Delta\nu P(\Delta\nu)\exp(j2\pi\Delta\nu t). \quad (23)$$

From Eq. (11), the second integral in Eq. (23) is by definition equal to $p(t)$. By applying Parseval's theorem, we obtain

$$\int_{-\infty}^{\infty} d\nu \langle |V(\nu)|^2 \rangle = \int_{-\infty}^{\infty} dt \langle |v(t)|^2 \rangle. \quad (24)$$

When Eq. (18) is used, together with Eqs. (23) and (24), the normalized ensemble average intensity temporal response is equal to the time-of-flight distribution for the scattered partial waves in the random medium and is given by

$$p(t) = \frac{\langle I(t) \rangle}{\int_{-\infty}^{\infty} dt \langle I(t) \rangle}. \quad (25)$$

E. Diffusion Approximation

The transport of light in a random medium in the weak-scattering limit (the transport mean free path is large compared with the wavelength) is well described by the Boltzmann transport equation, often called the radiative transfer equation (RTE) for light.^{1,33} The RTE models the transport of average intensity through the random medium, where the interference of partial waves along different paths can be neglected. In practice, the RTE is usually difficult to solve analytically, but in many circumstances, the transport of light in a random medium can be modeled by the diffusion approximation to the RTE.¹ The conditions for validity of the diffusion approximation require the sample size be large compared with the transport mean free path and the absorption length be much larger than the transport mean free path. As will be shown by experimental data, the diffusion approximation accurately describes the samples used in this study.

It should also be pointed out that the conditions required to obtain zero-mean circular complex Gaussian statistics to describe the speckle field are independent of those required for the diffusion approximation to be valid. For example, a slab of ground glass readily produces a scattered field with Gaussian statistics, but the light transport is not well described by the diffusion approximation. Therefore, the second-order and third-order correlation techniques discussed in Subsection 2.C are general and not limited to random media in the diffusion regime.

The diffusion equation governing the radiative flux density $\Phi(\mathbf{r}, t)$ (in units of W m^{-2}) is³⁴

$$\frac{\partial}{\partial t} \Phi(\mathbf{r}, t) + v\mu_a \Phi(\mathbf{r}, t) - \nabla \cdot D \nabla \Phi(\mathbf{r}, t) = vS_0(\mathbf{r}, t), \quad (26)$$

where v is the transport velocity, $D = v/3(\mu'_s + \mu_a)$ is the diffusion coefficient (in units of $\text{m}^2 \text{s}^{-1}$), μ'_s is the reduced scattering coefficient and μ_a is the absorption coefficient

(both in units of m^{-1}), and $S_0(\mathbf{r}, t)$ is the source. For validity of the diffusion approximation, $\mu'_s \gg \mu_a$. The transport mean free path is given by $1/(\mu'_s + \mu_a) \approx 1/\mu'_s$ for the materials that we have studied. The radiative current density $\mathbf{J}(\mathbf{r}, t)$ (in units of W m^{-2}) can be found under the diffusion approximation from Fick's law,³⁴ resulting in

$$\mathbf{J}(\mathbf{r}, t) = -\frac{D}{v} \nabla \Phi(\mathbf{r}, t). \quad (27)$$

The intensity temporal response of a random medium under the diffusion approximation is related to the Green's function for Eq. (26). We use a source term $S_0(\mathbf{r}, t) = \delta(\mathbf{r}', t)$, where \mathbf{r}' is the source location, to solve Eqs. (26) and (27) and obtain an expression for the radiative current density at a particular observation point. The intensity at the observation point measured by a photodetector is $I_D(t) = \hat{\mathbf{n}} \cdot \mathbf{J}$, where $\hat{\mathbf{n}}$ is the detector normal unit vector.³⁵ Normalizing this result gives

$$p_D(t) = \frac{I_D(t)}{\int_{-\infty}^{\infty} dt I_D(t)}, \quad (28)$$

which is identical in form to Eq. (25). Therefore the time-of-flight distribution for a random medium under the diffusion approximation can be found by using $p(t) = p_D(t)$. For a homogeneous slab of diffusely scattering random media, a quasi-analytic solution to the Green's function for Eq. (26) can be found by using image theory.^{8,36}

3. BISPECTRAL TECHNIQUE FOR RECONSTRUCTING THE TEMPORAL RESPONSE

A. Bispectral Theory

Third-order correlations provide many advantages over second-order correlations for signal recovery by allowing phase information about the underlying signal to be obtained, as reviewed by Lohmann and Wirnitzer.³⁰ Here it is shown that third-order frequency correlation measurements of speckle intensity permit the temporal response of a random medium to be reconstructed.

To review some of the basic concepts, we consider the arbitrary real signal $f(t)$ whose third-order temporal correlation is given by

$$g^{(3)}(\tau_1, \tau_2) = \int_{-\infty}^{\infty} dt f(t)f(t + \tau_1)f(t + \tau_2). \quad (29)$$

The Fourier transform of $g^{(3)}(\tau_1, \tau_2)$,

$$G^{(3)}(\nu_1, \nu_2) = \int_{-\infty}^{\infty} d\tau_1 \int_{-\infty}^{\infty} d\tau_2 g^{(3)}(\tau_1, \tau_2) \times \exp[-j2\pi(\nu_1\tau_1 + \nu_2\tau_2)], \quad (30)$$

is defined as the bispectrum of the function $f(t)$. The function $f(t)$ can be expressed in terms of its Fourier transform $F(\nu)$ by

$$f(t) = \int_{-\infty}^{\infty} dt F(\nu) \exp(j2\pi\nu t). \quad (31)$$

Substituting Eq. (31) into Eq. (29) allows the bispectrum of $f(t)$, defined in Eq. (30), to be written as

$$G^{(3)}(\nu_1, \nu_2) = F(\nu_1)F(\nu_2)F(-\nu_1 - \nu_2). \quad (32)$$

Since $f(t)$ is real, its Fourier transform is Hermitian, allowing the identity $F(-\nu_1 - \nu_2) = F^*(\nu_1 + \nu_2)$ to be used in Eq. (32), giving

$$G^{(3)}(\nu_1, \nu_2) = F(\nu_1)F(\nu_2)F^*(\nu_1 + \nu_2). \quad (33)$$

We shall express the Fourier transform of $f(t)$ in terms of its magnitude and phase as $F(\nu) = A(\nu)\exp[j\phi(\nu)]$, and the bispectrum in terms of its magnitude and phase as $G^{(3)}(\nu_1, \nu_2) = B(\nu_1, \nu_2)\exp[j\psi(\nu_1, \nu_2)]$. Then the relationship between the Fourier phase and the bispectral phase of $f(t)$, obtained from Eq. (33), is

$$\psi(\nu_1, \nu_2) = \phi(\nu_1) + \phi(\nu_2) - \phi(\nu_1 + \nu_2). \quad (34)$$

Equation (34) shows that the bispectral phase is a linear combination of Fourier phases. Also, if we add an arbitrary linear phase component to the Fourier phase of $f(t)$, replacing $\phi(\nu)$ by $\hat{\phi}(\nu) = \phi(\nu) + \alpha\nu$, then from Eq. (34), we see that the bispectral phase is independent of the linear phase component $\alpha\nu$. For this reason, the bispectrum of $f(t)$ is blind to linear Fourier phase. In the time domain, this equates to all real functions $f(t)$ that differ by an arbitrary time offset having the same bispectrum.

Equation (34) can be exploited to reconstruct the Fourier phase of $f(t)$ from its bispectral phase with a simple explicit scheme.³¹ Writing the Fourier and bispectral phases in discrete notation, where $\phi_k = \phi(k\delta\nu)$ is the k th Fourier phase and $\psi_{i,j} = \psi(i\delta\nu, j\delta\nu)$ is the (i, j) th component of the bispectral phase, where $\delta\nu$ is the sample frequency increment, allows the Fourier phase to be reconstructed by using³¹

$$\phi_k = \frac{1}{k-1} \sum_{i=1}^{k-1} \phi_i + \phi_{k-i} - \psi_{i,k-i}, \quad k = 2, \dots, N_s, \quad (35)$$

where $\phi_0 = 0$, $\phi_1 = \phi(\delta\nu)$ is arbitrary, and N_s is the number of samples. The arbitrary value for ϕ_1 gives the reconstructed Fourier phase 1 degree of freedom that is equivalent to an indeterminate linear Fourier phase, which in the time domain gives an arbitrary time offset. We apply this scheme in our work. Alternatively, writing Eq. (34) as an overdetermined system of linear equations for the unknown Fourier phase ϕ_k , we can apply a least-squares reconstruction technique.³⁷⁻³⁹

B. Reconstruction of the Temporal Response

From a comparison of Eqs. (15) and (33), the speckle intensity third-order frequency correlation from a random medium is equal to twice the real part of the bispectrum of the temporal response $p(t)$. Therefore, by using bispectral techniques, we can reconstruct the Fourier phase, and when this is combined with the Fourier magnitude obtained from the speckle intensity second-order frequency correlations in Eq. (14), we obtain the Fourier

transform of the temporal response, $P(\Delta\nu)$. Taking an inverse Fourier transform recovers the temporal response $p(t)$.

The normalized intensities $\tilde{I}_1 = \tilde{I}(\nu_0)$, $\tilde{I}_2 = \tilde{I}(\nu_0 + \Delta\nu_1)$, and $\tilde{I}_3 = \tilde{I}(\nu_0 + \Delta\nu_1 + \Delta\nu_2)$, when used in the third-order correlation in Eq. (15) and the second-order correlation in Eq. (14), allow the bispectral phase of $p(t)$ to be written as

$$\psi(\Delta\nu_1, \Delta\nu_2) = \pm \cos^{-1} \left[\frac{\langle \tilde{I}_1 \tilde{I}_2 \tilde{I}_3 \rangle}{2(\langle \tilde{I}_1 \tilde{I}_2 \rangle \langle \tilde{I}_2 \tilde{I}_3 \rangle \langle \tilde{I}_3 \tilde{I}_1 \rangle)^{1/2}} \right]. \quad (36)$$

The bispectral phase from Eq. (36) is then used with Eq. (34) to reconstruct the Fourier phase by the method of Eq. (35).

Note in Eq. (36) that the speckle correlation measurements provide only the cosine of the bispectral phase. The main consequence of this is a sign ambiguity in the total reconstructed Fourier phase, leading to time-reversal indeterminacy in the temporal response. This is not a severe limitation, provided that the bispectral phase does not rapidly change sign, which is the case when, for example, the Fourier phase is monotonic. In this case, we can take the inverse cosine operation in Eq. (36) to produce all positive (or all negative) values for the bispectral phase. The form of the temporal responses for the random media used in this study are all observed to have a monotonic Fourier phase.

4. EXPERIMENTAL RESULTS

A. Measured Speckle Patterns

The experimental setup used to obtain the speckle intensity frequency correlation data is shown in Fig. 1. The tunable laser source used was an external cavity (Littman–Metcalf design) laser diode that has a single-mode output with a narrow linewidth (nominally 5 MHz) and a center wavelength of $\lambda = 850$ nm. The output light from this source was linearly polarized with an average power of 10 mW. An optical isolator was used to prevent backreflections destabilizing the laser diode output. The center frequency can be tuned over a range of approximately 60 GHz. A small portion of the output power was coupled into a scanning Fabry–Perot interferometer, using the half-wave plate (HWP) retarder and polarizing beam-splitter (PBS) combination, to monitor the laser diode center frequency as it was tuned. Most of the optical power was focused onto the front face of the scattering random medium by the lens L1 of focal length $f_{L1} = 50$ mm. The random media used for this study were commercial white acrylics (Cryo Industries, Acrylite FF) that consist of a transparent acrylic background embedded with a homogeneous concentration of small TiO_2 particles approximately 50 nm in diameter.

A small area on the back face of the scattering random medium, approximately $1.2 \text{ mm} \times 1.5 \text{ mm}$ in size, was imaged onto a cooled CCD camera with 1000×800 pixels of size $15 \mu\text{m} \times 15 \mu\text{m}$. We assume stationary statistics over this area. The imaging optics consist of a spatial filter in a $4f$ telescope configuration that gives unity magnification at the plane P1 and a lens L2

that provides a magnification of $M = 10$ from the plane P1 to the CCD image plane. The spatial filter was formed from two identical achromatic lenses of focal length $f = 50$ mm and an adjustable iris aperture with a typical diameter of $D = 2$ mm, located at the Fourier focal plane. The aperture was used to control the spatial feature size in the random structure of a measured speckle pattern. The lens L2 was an achromatic lens of focal length $f_{L2} = 75$ mm.

The light emerging from the random medium was no longer linearly polarized on account of the multiple scattering. Therefore, the imaged scattered light was passed through a polarizer to analyze the same linear polarization as that of the input light for detection with the CCD camera, since a single linear polarization (scalar) model was assumed for the scattered field. Exposure times of approximately 1 s were used by the CCD camera to acquire a speckle image. A typical measured speckle intensity pattern is shown in Fig. 2.

We calculated the intensity histogram for the speckle image in Fig. 2, which is presented as a semilogarithmic plot in Fig. 3. This provides an estimate of the first-order statistics of the speckle intensity, and it closely models the ideal negative exponential probability density function for intensity expected for fully developed (circular complex Gaussian) speckle field statistics,⁴ which is given by

$$p_I(I) = \frac{1}{\langle I \rangle} \exp(-I/\langle I \rangle), \quad (37)$$

where the mean intensity is given by $\langle I \rangle$. However, there was a small intensity offset, η_I , which we have found to be well modeled by $\eta_I = \beta \langle I \rangle$, where $\beta = 0.13$ for our experimental setup. We could not eliminate this intensity offset, and we believe that it was scattered laser light entering the imaging domain, possibly from multiple reflections, and behaving as background light. It was not am-

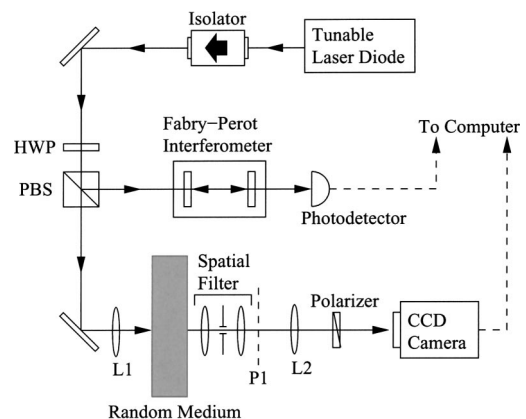


Fig. 1. Experimental setup used to measure the speckle intensity patterns as a function of the laser diode center frequency. The Fabry–Perot interferometer is used to monitor the change in the laser diode center frequency as it is tuned. Lens L1 ($f_{L1} = 50$ mm) focuses the laser output onto the front face of the scattering random medium. The spatial structure of the speckle pattern at plane P1 is controlled by the unity magnification spatial filter. Lens L2 ($f_{L2} = 75$ mm) provides a magnification factor of $M = 10$ from plane P1 to the CCD image plane, where the resultant frequency-dependent speckle pattern is obtained.

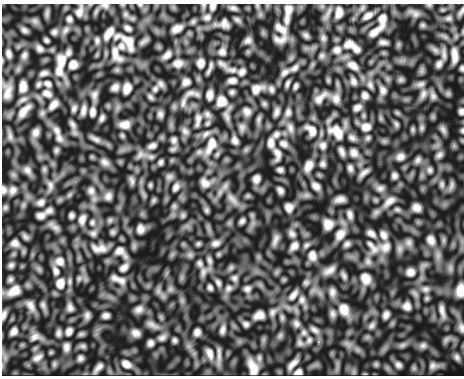


Fig. 2. Typical speckle image of the output intensity from the random medium obtained by the CCD.

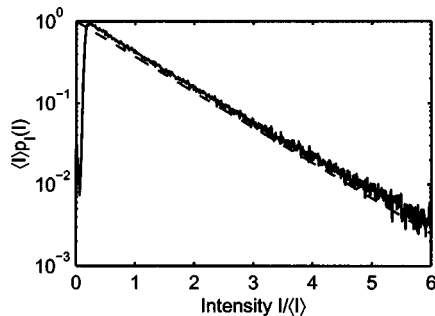


Fig. 3. Intensity histogram of the speckle pattern given in Fig. 2 plotted on a semilogarithmic scale (solid curve). Also shown is the ideal negative exponential intensity probability density function in Eq. (37) expected for zero-mean circular complex Gaussian field statistics (dashed curve).

bient light, since that was rigorously eliminated from the experiment, as confirmed by obtaining background (no laser light) images. We also found that it was sample independent, because we obtained the identical offset for a ground-glass reference sample and other random media with different scattering properties. For all subsequent measurements, we subtracted the intensity offset η_I from the intensity data before processing. This did not affect our frequency correlations because the offset behaved as a statistically independent background intensity. The dip seen in Fig. 3 for the low-intensity values is due to the combined effect of the small intensity offset and the read noise of the CCD camera. In a previous study,¹⁶ we did not observe such an intensity offset because it was masked by a small drift in the reference level of the analog-to-digital converter in the CCD camera.

Assuming that the speckle statistics are ergodic, we estimated the ensemble average quantities in Eqs. (14) and (15) by spatial sampling of the speckle intensity. To ensure accurate sampling of the underlying speckle field, the detection area (CCD pixel size) needs to be small compared with the width of the speckle intensity spatial autocorrelation function.^{40,41} The spatial autocorrelation function provides a measure of the average “speckle size” and is defined by⁴

$$R_I(\Delta r) = \frac{\langle I(r_0 + \Delta r)I(r_0) \rangle}{\langle I \rangle^2}, \quad (38)$$

where $I(r_0)$ is the speckle intensity at spatial location r_0 in the image plane and Δr is a small spatial offset. The speckle intensity spatial autocorrelation in Eq. (38) is dependent upon the point-spread function of the imaging optics and the spatial structure of the speckle field in the object plane.^{42,43} For our imaging optics shown in Fig. 1, we calculate $R_I(\Delta r)$ for a circular complex Gaussian field in the object plane whose spatial structure is very small compared with the point-spread function of the imaging optics using scalar diffraction theory under the Fresnel approximation:

$$R_I(\Delta r) = 1 + \left| 2 \frac{J_1\left(\frac{\pi D \Delta r}{M \lambda f}\right)}{\frac{\pi D \Delta r}{M \lambda f}} \right|^2, \quad (39)$$

where $J_1(x)$ is the Bessel function of the first kind and order 1. The calculated spatial autocorrelation function of the measured speckle image in Fig. 2 is plotted in Fig. 4, which is very accurately modeled by the theoretical result given by Eq. (39), for our imaging geometry with $f = 50$ mm, $D = 2$ mm, and $M = 10$. In this case, the speckles have an average diameter of $250 \mu\text{m}$, large compared with the CCD pixel area of $15 \mu\text{m} \times 15 \mu\text{m}$ that is required for accurate sampling of the speckle intensity.

To ensure accurate statistics, a large number of independent measurements are usually required. For our measurements, this equates to having a large number of independent speckles in an image obtained by the CCD. The number of independent samples is given not by the number of CCD pixels but by the ratio of the CCD area to the average area of an individual speckle. If we approximate the average speckle area by $250 \mu\text{m} \times 250 \mu\text{m}$ and compare this with the CCD imaging area of $15 \text{ mm} \times 12 \text{ mm}$, we have approximately 2880 independent intensity samples in a measured speckle pattern. This proved to be sufficient for estimating the ensemble statistics. Of course, one could make the speckle size smaller by increasing the aperture diameter D of the spatial filter in the imaging optics in Fig. 1. However, if the average speckle size begins to approach the CCD pixel size, then

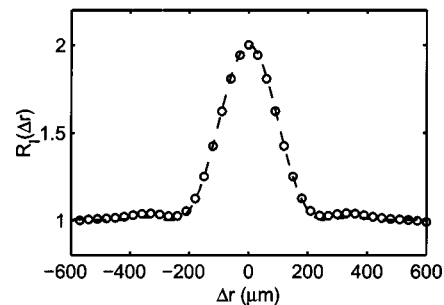


Fig. 4. Measured intensity spatial autocorrelation function of the speckle image shown in Fig. 2 (circles). The theoretical result in Eq. (39) is also plotted, showing good agreement (dashed curve). The average speckle diameter, taken as the distance from $\Delta r = 0$ to the first minimum, is estimated to be approximately $250 \mu\text{m}$.

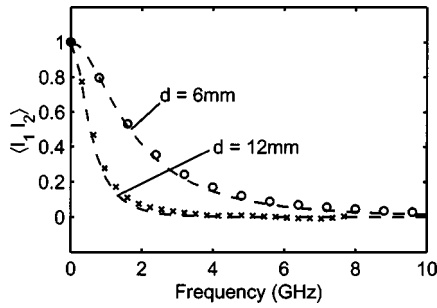


Fig. 5. Plot of the measured second-order intensity frequency correlation defined in Eq. (40) for two slab thicknesses of a scattering random medium (symbols). Excellent agreement with the second-order intensity correlation in Eq. (14), calculated with an analytic diffusion model for the temporal response $p(t)$, with values of $\mu'_s = 13\text{ cm}^{-1}$ and negligible absorption ($\mu_a = 0\text{ cm}^{-1}$) was obtained (dashed curves).

the speckle intensity will not be accurately sampled. We recommend that the average speckle size be 10–20 times that of the CCD pixel linear dimension.

B. Measured Frequency Correlations

Speckle images were measured for 25 discrete laser frequencies in order to calculate the intensity frequency correlations in Eqs. (14) and (15). These measurements were performed for two homogeneous sample thicknesses of $d = 6\text{ mm}$ and $d = 12\text{ mm}$. (The sample of thickness $d = 12\text{ mm}$ was made from two identical slabs of thickness $d = 6\text{ mm}$.) For the sample thickness of $d = 6\text{ mm}$, frequency increments of $\delta\nu = 1\text{ GHz}$ between each measured speckle pattern were used, and for the sample of thickness $d = 12\text{ mm}$, frequency increments of $\delta\nu = 0.4\text{ GHz}$ were used.

The second-order intensity correlation of Eq. (14) is dependent only upon the frequency difference between measurements. Therefore we averaged each frequency combination pair from the available data set that gave the same frequency difference to form the intensity second-order frequency correlation data point for that particular frequency difference. Denoting the normalized intensity sample at each frequency increment by $\tilde{I}_i = \tilde{I}(\nu + i\delta\nu)$ for $i = 0, 1, \dots, N - 1$, with $N = 25$, we then estimated the second-order correlation in Eq. (14), averaged over all possible combinations, by

$$\langle \tilde{I}(\nu)\tilde{I}(\nu + \Delta\nu) \rangle_{\text{meas}} = \frac{1}{N - i} \sum_{j=0}^{N-1-i} \langle \tilde{I}_j \tilde{I}_{j+i} \rangle, \quad (40)$$

with $\Delta\nu = i\delta\nu$ and $i = 0, 1, \dots, N - 1$. This averaging procedure will reduce the sampling error of the small frequency differences more than for the larger frequency differences because there are more frequency pairs to average. Of course, one may increase the range of the laser diode frequency scan to be much greater than the frequency range of interest, increasing the number of available frequency pairs used to form the average.

The results for the measured second-order intensity correlations in Eq. (40) are plotted in Fig. 5 for the two slab thicknesses of $d = 6\text{ mm}$ and $d = 12\text{ mm}$. Also plotted is the second-order intensity correlation in Eq. (14), evaluated by using the temporal response $p(t)$ cal-

culated from Eq. (28) under the diffusion approximation for a homogeneous slab and taking a Fourier transform to obtain the Fourier magnitude $|P(\Delta\nu)|$. There is very good agreement between our measured speckle correlations and the analytic diffusion model, with $\mu'_s = 13\text{ cm}^{-1}$ and negligible absorption ($\mu_a = 0\text{ cm}^{-1}$) for each slab thickness d .

To calculate the third-order intensity correlation in Eq. (15), we averaged each frequency triplet from the available data set of measured intensities that gave the same frequency differences for $\Delta\nu_1$ and $\Delta\nu_2$ to form each measured third-order correlation data point. Averaging all possible combinations gives the measured third-order correlation

$$\langle \tilde{I}(\nu)\tilde{I}(\nu + \Delta\nu_1)\tilde{I}(\nu + \Delta\nu_1 + \Delta\nu_2) \rangle_{\text{meas}} = \frac{1}{N - i - j} \sum_{k=0}^{N-1-i-j} \langle \tilde{I}_k \tilde{I}_{k+i} \tilde{I}_{k+i+j} \rangle, \quad (41)$$

where $\Delta\nu_1 = i\delta\nu$, $\Delta\nu_2 = j\delta\nu$, and $i, j = 0, 1, \dots, N - 1$, with $i + j \leq N - 1$. Figure 6 shows a plot of the third-order intensity correlation of the measured data for the homogeneous slab of thickness $d = 6\text{ mm}$.

C. Reconstructed Temporal Response

To reconstruct the temporal response of a random medium, we first determined the Fourier magnitude by using second-order correlations, and second, calculated the Fourier phase from third-order correlations; then we combined these results and performed an inverse Fourier transform. Figure 7(a) shows the reconstructed Fourier magnitude for the two sample thicknesses. The Fourier magnitude is related to the second-order intensity correlation by Eq. (14) and was obtained by taking the square root of the measured second-order correlation calculated by Eq. (40) and shown in Fig. 5. The reconstructed Fourier phase is plotted in Fig. 7(b) for both sample thicknesses. We obtained this result by using the measured second-order and third-order correlations in Eqs. (40) and (41) in Eq. (36) to estimate the bispectral phase. Then we calculated the Fourier phase from the bispectral phase

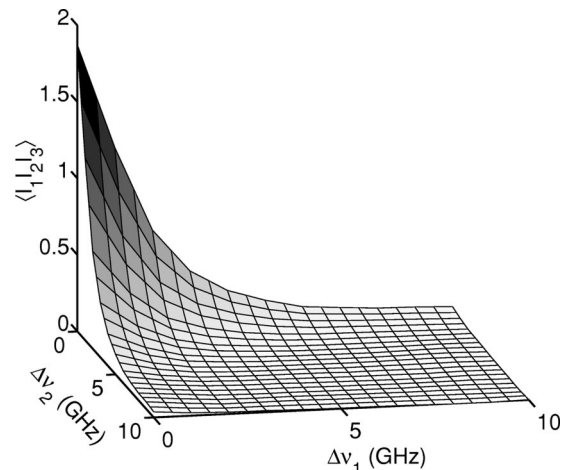


Fig. 6. Plot of the measured third-order intensity correlation defined by Eq. (41) for the sample of thickness $d = 6\text{ mm}$. These data are equal to twice the real part of the bispectrum of $p(t)$.

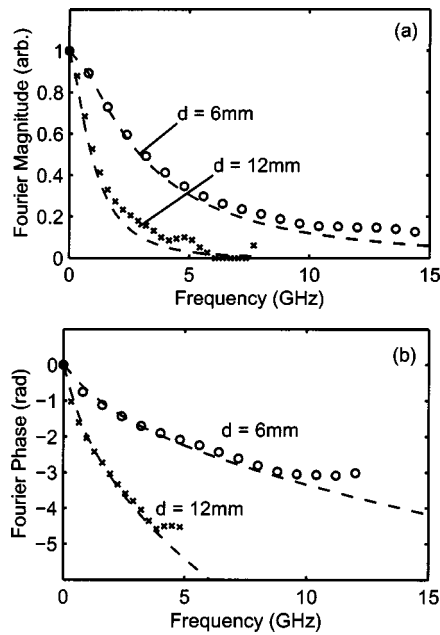


Fig. 7. (a) Reconstructed Fourier magnitude of the temporal response for the two sample thicknesses with the use of measured data (symbols) and the Fourier magnitude calculated with an analytic diffusion model for the temporal response with $\mu_s' = 13 \text{ cm}^{-1}$ and $\mu_a = 0 \text{ cm}^{-1}$ for each thickness (dashed curves). (b) Reconstructed Fourier phase of the temporal response with the use of measured data (symbols) and the Fourier phase calculated with the diffusion model for each sample thickness (dashed curves).

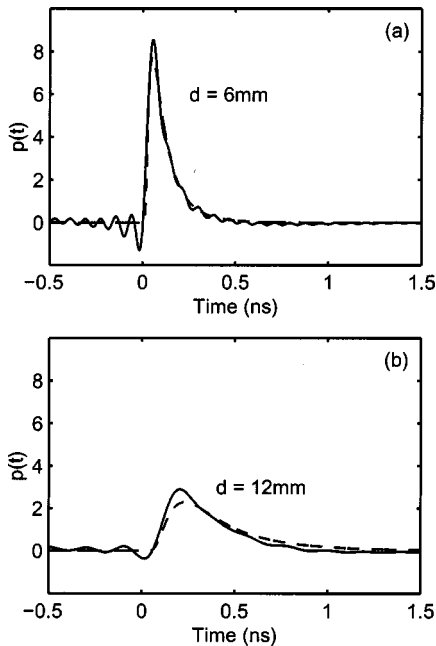


Fig. 8. Reconstructed temporal response obtained by taking an inverse fast Fourier transform of the Fourier magnitude and phase data presented in Fig. 7 (solid curves). Each sample thickness gives excellent agreement with a diffusion approximation model for the temporal response (dashed curves).

by using Eq. (35). The arbitrary linear phase was chosen to overlap the reconstructed Fourier phase with the Fourier phase obtained from using an analytic diffusion approximation solution for the temporal response, which is also shown in Fig. 7(b).

There is a noticeable deviation of the reconstructed Fourier phases from the analytic results for the diffusion approximation above approximately 12 GHz for the sample thickness of $d = 6 \text{ mm}$ and above 5 GHz for the sample thickness of $d = 12 \text{ mm}$. This is due to the measured second-order and third-order intensity correlations becoming very small and susceptible to experimental noise, thus causing errors in the bispectral phase calculated by using Eq. (36).

We applied an inverse fast Fourier transform to the reconstructed Fourier magnitude and phase data, giving the reconstructed temporal responses shown in Fig. 8(a) for the sample thickness of $d = 6 \text{ mm}$ and in Fig. 8(b) for the sample thickness of $d = 12 \text{ mm}$. These results agree very well with those expected from the diffusion approximation model. We can also see that the width of the temporal response scales with sample thickness in a manner predicted by a diffusion approximation model. The oscillations in the reconstructed temporal response are artifacts due to the finite frequency range over which the Fourier phase was reconstructed. With reference to Fig. 7(b), a bandwidth of 12 GHz was used for the sample of thickness $d = 6 \text{ mm}$, and of 5 GHz for the sample of thickness $d = 12 \text{ mm}$.

D. Direct Measurement of Intensity Temporal Response

We confirmed the validity of the temporal response obtained with third-order speckle correlations by directly measuring with a streak camera the intensity temporal response defined in Eq. (25). An ultrafast mode-locked Ti:sapphire laser with a pulse width of approximately 200 fs was used as the input excitation. The center wavelength of the laser was 835 nm, which is a 2% difference in wavelength from the 850 nm used for the speckle frequency correlation experiments. This small difference in wavelength will cause a slight change in the scattering properties of the random medium (approximately 7% based on the λ^{-4} dependence of Rayleigh scattering). The data show that these effects are minimal, and we shall neglect this small difference.

A streak camera was used to obtain the intensity temporal response data. The imaging optics used for the streak camera measurements are different from the configuration shown in Fig. 1 for the speckle measurements. A single achromatic lens, of focal length 50 mm, was used with an adjustable iris aperture of diameter 4 mm, placed at the lens. The lens was positioned to give a magnification factor of 10 from the object plane (output face of the random medium sample) to the image plane (5-mm \times 60- μm input slit of the streak camera). This permitted us to collect sufficient light from a small area on the output face of the random medium. Figure 9(a) shows the measured streak camera data for the sample of thickness $d = 6 \text{ mm}$, with the reconstructed result from the third-order speckle correlation technique overlaid. The measured streak camera data for the sample of thickness $d = 12 \text{ mm}$ are shown in Fig. 9(b). These results clearly show that the two measurement techniques are in excellent agreement.

E. Inhomogeneous Sample Measurements

We also measured second-order and third-order speckle correlations for an inhomogeneous sample, whose cross

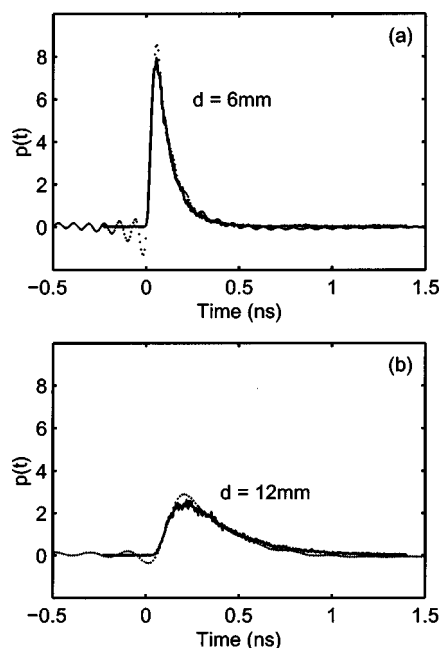


Fig. 9. Plots of the intensity temporal response [Eq. (25)] directly measured with a streak camera for each sample thickness (solid curves). Overlaid are the temporal responses reconstructed by using third-order speckle correlations, given in Fig. 8, showing excellent agreement (dotted curves).

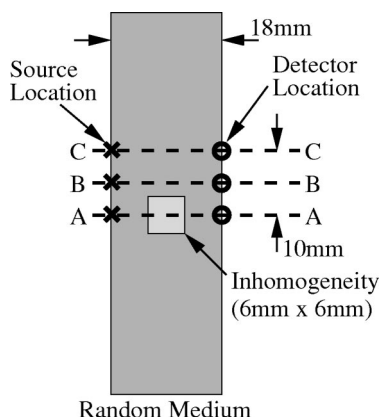


Fig. 10. Cross section of inhomogeneous random medium sample. The background has a scattering coefficient of $\mu'_s = 13 \text{ cm}^{-1}$, and the lower-scattering inhomogeneity has an estimated scattering coefficient of $\mu'_s = 4 \text{ cm}^{-1}$. The source-detector location combinations used are A-A, B-B, and C-C, each separated by 5 mm.

section is shown in Fig. 10. This sample, of total thickness 18 mm, was constructed from three sheets of thickness 6 mm and area $140 \text{ mm} \times 140 \text{ mm}$ of the same scattering white acrylic (with $\mu'_s = 13 \text{ cm}^{-1}$) as that used for the previous measurements, which provided the data for Figs. 2–9. Centrally located within the background material was an inhomogeneity with cross-sectional dimensions of $6 \text{ mm} \times 6 \text{ mm}$ and a length of 140 mm. This inhomogeneity was lower in scattering than the background material and was also a white acrylic but with an estimated scattering coefficient of $\mu'_s = 4 \text{ cm}^{-1}$.

Three source-detector location combinations were used for measuring speckle correlation data and are shown in

Fig. 10. The first source-detector location combination, denoted by A-A, was centrally located about the inhomogeneity. The second combination, denoted by B-B, was offset by 5 mm from A-A, and its “line of sight” did not pass through the inhomogeneity. The third combination, denoted by C-C, was offset by 10 mm from A-A.

The second-order intensity correlation measurements for the three source-detector locations are shown in Fig. 11(a). The difference in the second-order intensity correlation for each source-detector location is seen to be small, but they display the correct trend for each plot as a function of frequency; the source-detector location A-A encounters a greater volume of the lower-scattering inhomogeneity than source-detector combination C-C, and thus it will have a broader second-order intensity correlation as a function of frequency. The source detector combination B-B is geometrically between A-A and C-C, with intermediate influence of the lower-scattering inhomogeneity, and hence the second-order intensity correlation as a function of frequency for B-B lies between the results for A-A and C-C, as also seen in Fig. 11(a). The temporal responses for two source-detector locations are shown in Fig. 11(b), which were reconstructed by using both the second-order and third-order intensity correlations. We expect that the temporal response for each source-detector location will be different, since the time-of-flight distributions will be different on account of the inhomogeneous distribution of scattering properties. For the source-detector location A-A, the presence of the lower-scattering inhomogeneity will provide a greater volume of lower-scattering paths than for the C-C source-detector location; thus we expect the time-of-flight distri-

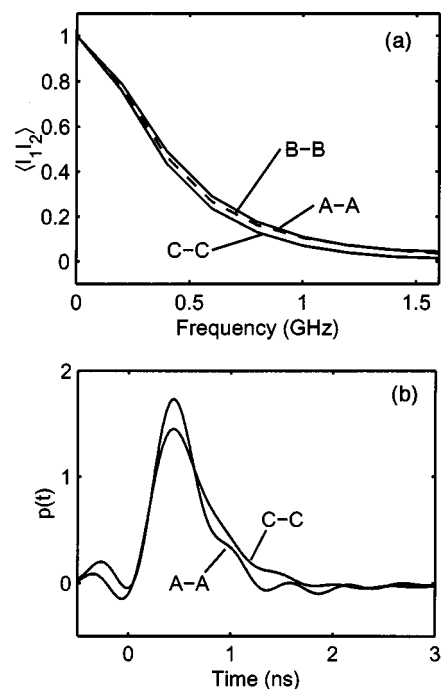


Fig. 11. (a) Measured second-order intensity correlations for the inhomogeneous sample shown in Fig. 10 for the source-detector location combinations A-A, B-B, and C-C. (b) Reconstructed temporal responses for the inhomogeneous sample for the source-detector locations A-A and C-C.

bution for A–A to be narrower than that for C–C, hence giving a narrower temporal response, as seen in Fig. 11(b).

5. CONCLUSIONS

We have shown that the proposed third-order speckle intensity correlation technique can be used to obtain the temporal response of a random medium with circular complex Gaussian field statistics. Second-order intensity correlations can provide information only about the Fourier magnitude of the temporal response, whereas third-order intensity correlations allow the Fourier phase of the temporal response to be determined. Use of the third-order correlation obviates the need for fitting parameters in a forward model for determining the temporal response. The measured data give results that are in excellent agreement with the direct measurement of the intensity temporal response obtained with a streak camera. We have also shown that the speckle intensity correlation measurements are sensitive to inhomogeneities within a homogeneous scattering domain and hence produce data that could be useful for image reconstruction within scattering media.

APPENDIX A: DEVELOPMENT OF FIELD STATISTICS

1. Jointly Gaussian Statistics

In this appendix, we develop the joint statistics of the scattered field from a random medium. We shall show that under assumptions (i)–(iii) given in Subsection 2.A, the scattered fields measured at different frequencies have zero-mean circular complex Gaussian joint statistics.

We desire to determine the joint statistics of the output field at frequencies $\nu_1, \nu_2, \dots, \nu_M$. Using Eq. (3), we obtain the output field of a random medium at frequency ν_m , for $m = 1, 2, \dots, M$:

$$E_o(\nu_m) = \frac{1}{\sqrt{N}} \sum_{k=1}^N A_k \exp[-j\phi_k(\nu_m)]. \quad (\text{A1})$$

We express the k th elementary phasor of this sum in terms of its real and imaginary components, given by $x_k(\nu_m) = A_k \cos \phi_k(\nu_m)$ and $y_k(\nu_m) = -A_k \sin \phi_k(\nu_m)$, respectively. For each frequency ν_m , Goodman⁴ has shown, by using assumptions (i)–(iii) and applying the central limit theorem, that these real and imaginary components of $E_o(\nu_m)$ are distributed as zero-mean Gaussian random variables. However, having *marginal* Gaussian statistics for each frequency does not imply that real and imaginary components for all frequencies $\nu_1, \nu_2, \dots, \nu_M$ are described by *jointly* Gaussian statistics.⁴⁴

To show that the statistics of the $E_o(\nu_m)$ are jointly Gaussian, we apply a multivariate form of the central limit theorem given by Berger⁴⁵ (see also Papoulis,⁴⁴ Billingsley,⁴⁶ and Middleton⁴⁷). Let $\mathbf{u}_1, \mathbf{u}_2, \dots, \mathbf{u}_N$ be a sequence of real, zero-mean, independent, and identically distributed random vectors of dimension $2M$ with finite second moments ($\langle \|\mathbf{u}_k\|^2 \rangle < \infty$, where $\|\cdot\|^2$ is the 2-norm) and covariance matrix \mathbf{C}_u . The random vector \mathbf{u} formed by

$$\mathbf{u} = \lim_{N \rightarrow \infty} \frac{1}{\sqrt{N}} \sum_{k=1}^N \mathbf{u}_k \quad (\text{A2})$$

will have the Gaussian joint probability density function

$$p_u(\mathbf{u}) = \frac{1}{(2\pi)^M |\mathbf{C}_u|^{1/2}} \exp\left(-\frac{1}{2} \mathbf{u}^T \mathbf{C}_u^{-1} \mathbf{u}\right). \quad (\text{A3})$$

After the $E_o(\nu_m)$ are related to \mathbf{u} , it therefore suffices to demonstrate a finite second moment in order to show the jointly Gaussian nature of the $E_o(\nu_m)$.

To show that the real and imaginary components of Eq. (A1) are jointly Gaussian for the frequencies $\nu_1, \nu_2, \dots, \nu_M$, we form the vectors $\mathbf{u}_1, \mathbf{u}_2, \dots, \mathbf{u}_N$ from the real and imaginary components of $E_o(\nu_m)$ as

$$\mathbf{u}_1 = \begin{pmatrix} x_1(\nu_1) \\ \vdots \\ x_1(\nu_M) \\ y_1(\nu_1) \\ \vdots \\ y_1(\nu_M) \end{pmatrix}, \quad \mathbf{u}_2 = \begin{pmatrix} x_2(\nu_1) \\ \vdots \\ x_2(\nu_M) \\ y_2(\nu_1) \\ \vdots \\ y_2(\nu_M) \end{pmatrix}, \dots, \quad (\text{A4})$$

$$\mathbf{u}_N = \begin{pmatrix} x_N(\nu_1) \\ \vdots \\ x_N(\nu_M) \\ y_N(\nu_1) \\ \vdots \\ y_N(\nu_M) \end{pmatrix}.$$

Let the covariance matrix \mathbf{C}_u be partitioned into submatrices:

$$\mathbf{C}_u = \begin{bmatrix} \mathbf{C}_{xx} & \mathbf{C}_{xy} \\ \mathbf{C}_{yx} & \mathbf{C}_{yy} \end{bmatrix}. \quad (\text{A5})$$

The (i, j) th element of \mathbf{C}_{pq} is given by $[\mathbf{C}_{pq}]_{i,j} = \langle p(\nu_i)q(\nu_j) \rangle$, where $p = x, y$ and $q = x, y$.

From assumptions (i)–(iii), the random vectors formed in Eq. (A4) have $\langle \mathbf{u}_k \rangle = 0$ for all k . Consider the vector norm

$$\|\mathbf{u}_k\|^2 = \sum_{m=1}^M A_k^2 \cos^2 \phi_k(\nu_m) + \sum_{m=1}^M A_k^2 \sin^2 \phi_k(\nu_m). \quad (\text{A6})$$

Taking the expected value of this vector norm and using assumption (iii) and the statistical independence of the k th random magnitude and random phase gives

$$\langle \|\mathbf{u}_k\|^2 \rangle = \sum_{m=1}^M \langle A_k^2 \rangle \langle \cos^2 \phi_k(\nu_m) \rangle + \sum_{m=1}^M \langle A_k^2 \rangle \langle \sin^2 \phi_k(\nu_m) \rangle. \quad (\text{A7})$$

By assumption (ii), the phase is uniformly distributed over the interval $-\pi$ to π , resulting in $\langle \cos^2 \phi_k(\nu_m) \rangle = 1/2$ and $\langle \sin^2 \phi_k(\nu_m) \rangle = 1/2$. Furthermore, by assumption (i), the random magnitudes A_k are identically distributed, giving $\langle A_k^2 \rangle = \langle A^2 \rangle$. Using these results gives

$$\langle \|\mathbf{u}_k\|^2 \rangle = M \langle A^2 \rangle. \quad (\text{A8})$$

From Eq. (7), the quantity $\langle A^2 \rangle$ is equal to the ensemble average intensity $\langle I \rangle$, which is finite by definition. Thus the second moment $\langle \|\mathbf{u}_k\|^2 \rangle$ is also finite. Therefore, by

the multivariate central limit theorem, the scattered field from a random medium $E_o(\nu_m)$ at frequencies ν_m has zero-mean jointly Gaussian statistics.

2. Circular Complex Gaussian Statistics

When the covariance matrix in Eq. (A5) has a special structure, the jointly Gaussian real random vector of length $2M$ can be conveniently represented as a *circular complex Gaussian random vector* of length M . The conditions for this are^{27,44}

$$\mathbf{C}_{xx} = \mathbf{C}_{yy}, \quad \mathbf{C}_{yx} = -\mathbf{C}_{xy}. \quad (\text{A9})$$

Forming the complex vector

$$\mathbf{z} = \begin{pmatrix} x(\nu_1) + jy(\nu_1) \\ \vdots \\ x(\nu_M) + jy(\nu_M) \end{pmatrix}, \quad (\text{A10})$$

we can define a complex covariance matrix \mathbf{C}_z whose (i, j) th element is given by $[\mathbf{C}_z]_{i,j} = \langle z(\nu_i)z^*(\nu_j) \rangle$. When Eqs. (A9) hold, $\mathbf{C}_z = 2(\mathbf{C}_{xx} - j\mathbf{C}_{xy})$. Under these conditions, the joint probability density function for the complex random vector \mathbf{z} can be written as⁴⁴

$$p_z(\mathbf{z}) = \frac{1}{\pi^M |\mathbf{C}_z|} \exp(-\mathbf{z}^H \mathbf{C}_z^{-1} \mathbf{z}), \quad (\text{A11})$$

where \mathbf{z}^H is the complex Hermitian transpose of \mathbf{z} . Further discussion on this form for the joint probability density function is given by Wooding⁴⁸ and Grettenberg.⁴⁹

To show that the statistics of the output fields $E_o(\nu_m)$ given by Eq. (A1) at frequencies ν_m from a random medium are circular complex Gaussian, we need to show that under assumptions (i)–(iii) the conditions given by Eqs. (A9) hold. Consider the (i, j) th element of \mathbf{C}_{xx} :

$$\langle x(\nu_i)x(\nu_j) \rangle = \frac{1}{N} \sum_{k=1}^N \sum_{l=1}^N \langle A_k A_l \cos \phi_k(\nu_i) \cos \phi_l(\nu_j) \rangle. \quad (\text{A12})$$

Since the random magnitudes and the random phases are assumed statistically independent, we can write

$$\begin{aligned} \langle x(\nu_i)x(\nu_j) \rangle &= \frac{1}{N} \sum_{k=1}^N \langle A_k^2 \rangle \langle \cos \phi_k(\nu_i) \cos \phi_k(\nu_j) \rangle \\ &+ \frac{1}{N} \sum_{k=1}^N \sum_{\substack{l=1 \\ l \neq k}}^N \langle A_k \rangle \langle A_l \rangle \langle \cos \phi_k(\nu_i) \rangle \\ &\times \langle \cos \phi_l(\nu_j) \rangle. \end{aligned} \quad (\text{A13})$$

Under assumption (ii), the random phase is uniformly distributed from $-\pi$ to π , and the second summation term in Eq. (A13) is equal to zero. If we relate the random phase to the random time of flight, as given by Eq. (4), and expand the cosine product by using a trigonometry identity, Eq. (A13) becomes

$$\begin{aligned} \langle x(\nu_i)x(\nu_j) \rangle &= \frac{1}{2N} \sum_{k=1}^N \langle A_k^2 \rangle [\langle \cos 2\pi(\nu_i - \nu_j)t_k \rangle \\ &+ \langle \cos 2\pi(\nu_i + \nu_j)t_k \rangle]. \end{aligned} \quad (\text{A14})$$

The second ensemble average cosine term is equal to zero, because if the phases $2\pi\nu_i t_k$ and $2\pi\nu_j t_k$ are each assumed uniform over $-\pi$ to π when taken mod 2π , then so is the phase $2\pi(\nu_i + \nu_j)t_k$. (See the discussion in Subsection 2.A.) However, we cannot make the same assumption about the phase $2\pi(\nu_i - \nu_j)t_k$, because the value of $\nu_i - \nu_j$ may not be large when compared with the range of values for t_k . Finally, since the random magnitudes are identically distributed and the random times of flight are identically distributed, we obtain the result

$$\langle x(\nu_i)x(\nu_j) \rangle = \langle A^2 \rangle \langle \cos 2\pi(\nu_i - \nu_j)t \rangle / 2. \quad (\text{A15})$$

Likewise, the (i, j) th elements of \mathbf{C}_{yy} , \mathbf{C}_{xy} , and \mathbf{C}_{yx} become

$$\langle y(\nu_i)y(\nu_j) \rangle = \langle A^2 \rangle \langle \cos 2\pi(\nu_i - \nu_j)t \rangle / 2, \quad (\text{A16})$$

$$\langle x(\nu_i)y(\nu_j) \rangle = \langle A^2 \rangle \langle \sin 2\pi(\nu_i - \nu_j)t \rangle / 2, \quad (\text{A17})$$

$$\langle y(\nu_i)x(\nu_j) \rangle = -\langle A^2 \rangle \langle \sin 2\pi(\nu_i - \nu_j)t \rangle / 2. \quad (\text{A18})$$

Thus the expressions given in Eqs. (A15)–(A18) satisfy the conditions in Eqs. (A9) for all i, j . Therefore the output fields $E_o(\nu_m)$ for frequencies ν_m from a random medium have circular complex Gaussian statistics under assumptions (i)–(iii). This permits use of the Gaussian moment theorem of Reed²⁸ for calculating all moments of the random output field.

APPENDIX B: FIELD CORRELATION

This appendix rigorously develops the expression for the field second-order correlation in Eq. (10), first demonstrated by Genack,²⁹ utilizing assumptions (i)–(iii) presented in Subsection 2.A. Using the random phasor sum model for the scattered field [Eq. (3)], we write the output field at frequency $\nu + \Delta\nu$ as

$$E_o(\nu + \Delta\nu) = \frac{1}{\sqrt{N}} \sum_{k=1}^N A_k \exp[-j\phi_k(\nu + \Delta\nu)], \quad (\text{B1})$$

where the random phase of the k th elementary partial wave is given by Eq. (4), as $\phi_k(\nu + \Delta\nu) = 2\pi(\nu + \Delta\nu)t_k$. Here t_k represents the random time of flight for the k th partial wave. Similarly, we write the output field at frequency ν as

$$E_o(\nu) = \frac{1}{\sqrt{N}} \sum_{l=1}^N A_l \exp[-j\phi_l(\nu)], \quad (\text{B2})$$

with the random phase of the l th elementary partial wave of $\phi_l(\nu) = 2\pi\nu t_l$. With the use of Eqs. (B1) and (B2), the second-order field correlation is

$$\begin{aligned} \langle E_o(\nu + \Delta\nu)E_o^*(\nu) \rangle &= \frac{1}{N} \sum_{k=1}^N \sum_{l=1}^N \langle A_k A_l \\ &\times \exp[-j\phi_k(\nu + \Delta\nu) + j\phi_l(\nu)] \rangle. \end{aligned} \quad (\text{B3})$$

Utilizing the statistical independence of the random magnitudes and the random phases and separating the summation into the two cases $k = l$ and $k \neq l$ results in

$$\begin{aligned}
\langle E_o(\nu + \Delta\nu)E_o^*(\nu) \rangle &= \frac{1}{N} \sum_{k=1}^N \langle A_k^2 \rangle \langle \exp[-j\phi_k(\nu + \Delta\nu) \\
&\quad + j\phi_k(\nu)] \rangle + \frac{1}{N} \sum_{k=1}^N \sum_{\substack{l=1 \\ l \neq k}}^N \langle A_k \rangle \langle A_l \rangle \\
&\quad \times \langle \exp(-j\phi_k(\nu + \Delta\nu)) \rangle \\
&\quad \times \langle \exp(j\phi_l(\nu)) \rangle. \quad (\text{B4})
\end{aligned}$$

Since the random phase is assumed uniformly distributed over $-\pi$ to π , the second summation in Eq. (B4) is zero. Also, since the elementary random magnitudes A_k are assumed to be identically distributed, as are the random times of flight t_k , Eq. (B4) becomes

$$\langle E_o(\nu + \Delta\nu)E_o^*(\nu) \rangle = \langle A^2 \rangle \langle \exp(-j2\pi\Delta\nu t) \rangle. \quad (\text{B5})$$

By definition, the expected value of the exponential term in Eq. (B5), with probability density function $p(t)$ for the random times of flight, is

$$\begin{aligned}
\langle \exp(-j2\pi\Delta\nu t) \rangle &= \int_{-\infty}^{\infty} dt p(t) \exp(-j2\pi\Delta\nu t) \\
&= P(\Delta\nu), \quad (\text{B6})
\end{aligned}$$

where $P(\Delta\nu)$ is the Fourier transform of $p(t)$. Finally, using Eq. (7), we obtain

$$\langle E_o(\nu + \Delta\nu)E_o^*(\nu) \rangle = \langle I \rangle P(\Delta\nu). \quad (\text{B7})$$

ACKNOWLEDGMENT

This work was supported by the National Science Foundation under contracts 9901907-ECS and 0203240-ECS.

Corresponding author K. J. Webb can be reached by e-mail at webb@purdue.edu.

REFERENCES

1. A. Ishimaru, *Wave Propagation and Scattering in Random Media* (Academic, New York, 1978).
2. V. V. Tuchin, in *Tissue Optics: Light Scattering Methods and Instruments for Medical Diagnosis*, Vol. TT38 of Tutorial Texts in Optical Engineering, D. C. O'Shea, ed. (SPIE Press, Bellingham, Wash., 2000).
3. M. C. W. van Rossum and T. M. Nieuwenhuizen, "Multiple scattering of classical waves: microscopy, mesoscopy, and diffusion," *Rev. Mod. Phys.* **71**, 313–371 (1999).
4. J. Goodman, "Statistical properties of laser speckle patterns," in *Laser Speckle and Related Phenomena*, 2nd ed., J. C. Dainty, ed. (Springer-Verlag, Berlin, 1984).
5. G. Parry, "Some effects of temporal coherence on the first order statistics of speckle," *Opt. Acta* **21**, 763–772 (1974).
6. T. Bellini, M. A. Glaser, and N. A. Clark, "Effects of finite laser coherence in quasielastic multiple scattering," *Phys. Rev. A* **44**, 5215–5223 (1991).
7. A. Z. Genack, "Optical transmission in disordered media," *Phys. Rev. Lett.* **58**, 2043–2046 (1987).
8. C. A. Thompson, K. J. Webb, and A. M. Weiner, "Diffusive media characterization using laser speckle," *Appl. Opt.* **36**, 3726–3734 (1997).
9. C. A. Thompson, K. J. Webb, and A. M. Weiner, "Imaging in scattering media by use of laser speckle," *J. Opt. Soc. Am. A* **14**, 2269–2277 (1997).
10. J. D. McKinney, M. A. Webster, K. J. Webb, and A. M. Weiner, "Characterization and imaging in optically scattering media by use of laser speckle and a variable-coherence source," *Opt. Lett.* **25**, 4–6 (2000).
11. J. C. Hebden and D. T. Delpy, "Enhanced time-resolved imaging with a diffusion model of photon transport," *Opt. Lett.* **19**, 311–313 (1994).
12. J. C. Hebden, S. R. Arridge, and D. T. Delpy, "Optical imaging in medicine: I. Experimental techniques," *Phys. Med. Biol.* **42**, 825–840 (1997).
13. B. B. Das, F. Liu, and R. R. Alfano, "Time-resolved fluorescence and photon migration studies in biomedical and model random media," *Rep. Prog. Phys.* **60**, 227–292 (1997).
14. J. C. Ye, K. J. Webb, C. A. Bouman, and R. P. Millane, "Optical diffusion tomography using iterative coordinate descent optimization in a Bayesian framework," *J. Opt. Soc. Am. A* **16**, 2400–2412 (1999).
15. A. B. Milstein, S. Oh, J. S. Reynolds, K. J. Webb, C. A. Bouman, and R. P. Millane, "Three-dimensional Bayesian optical diffusion tomography with experimental data," *Opt. Lett.* **27**, 95–97 (2002).
16. M. A. Webster, K. J. Webb, and A. M. Weiner, "Temporal response of a random medium from third-order laser speckle frequency correlations," *Phys. Rev. Lett.* **88**, 033901 (2002).
17. A. Z. Genack and J. M. Drake, "Relationship between optical intensity, fluctuations and pulse propagation in random media," *Europhys. Lett.* **11**, 331–336 (1990).
18. R. Hanbury Brown and R. Q. Twiss, "A new type of interferometer for use in radio astronomy," *Philos. Mag.* **45**, 663–682 (1954).
19. H. Gamo, "Triple correlator of photoelectric fluctuations as a spectroscopic tool," *J. Appl. Phys.* **34**, 875–876 (1963).
20. H. Gamo, "Phase determination of coherence functions by the intensity interferometer," in *Electromagnetic Theory and Antennas*, Vol. 6 of International Series of Monographs on Electromagnetic Waves, E. C. Jordan, ed. (Pergamon, New York, 1963), pp. 801–810.
21. A. W. Lohmann, G. Weigelt, and B. Wirtzner, "Speckle masking in astronomy: triple correlation theory and applications," *Appl. Opt.* **22**, 4028–4037 (1983).
22. E. I. Blount and J. R. Klauder, "Recovery of laser intensity from correlation data," *J. Appl. Phys.* **40**, 2874–2875 (1969).
23. S. Feng, C. Kane, P. A. Lee, and A. D. Stone, "Correlations and fluctuations of coherent wave transmissions through disordered media," *Phys. Rev. Lett.* **61**, 834–837 (1988).
24. S. Feng and P. A. Lee, "Mesoscopic conductors and correlations in laser speckle patterns," *Science* **251**, 633–639 (1991).
25. J. H. Li and A. Z. Genack, "Correlation in laser speckle," *Phys. Rev. E* **49**, 4530–4533 (1994).
26. F. Scheffold, W. Hartl, G. Maret, and E. Matijevic, "Observation of long-range correlations in temporal intensity fluctuations in light," *Phys. Rev. B* **56**, 10942–10952 (1997).
27. J. W. Goodman, *Statistical Optics* (Wiley, New York, 1985).
28. I. S. Reed, "On a moment theorem for complex Gaussian processes," *IRE Trans. Inf. Theory* **IT-8**, 194–195 (1962).
29. A. Z. Genack, "Fluctuations, correlations and average transport of electromagnetic radiation in random media," in *Scattering and Localization of Classical Waves in Random Media*, P. Sheng, ed. (World Scientific, Singapore, 1990), pp. 207–311.
30. A. W. Lohmann and B. Wirtzner, "Triple correlations," *Proc. IEEE* **72**, 889–901 (1984).
31. H. Bartelt, A. W. Lohmann, and B. Wirtzner, "Phase and amplitude recovery from bispectra," *Appl. Opt.* **23**, 3121–3129 (1984).
32. J. D. Gaskill, *Linear Systems, Fourier Transforms, and Optics* (Wiley, New York, 1978).
33. R. Pnini and B. Shapiro, "Fluctuations in transmission of waves through disordered slabs," *Phys. Rev. B* **39**, 6986–6994 (1989).
34. J. J. Duderstadt and L. J. Hamilton, *Nuclear Reactor Analysis* (Wiley, New York, 1976).
35. R. C. Haskell, L. O. Svaasand, T. T. Tsay, T. C. Feng, M. S. McAdams, and B. J. Tromberg, "Boundary conditions for the diffusion equation in radiative transfer," *J. Opt. Soc. Am. A* **11**, 2727–2741 (1994).
36. M. S. Patterson, B. Chance, and B. C. Wilson, "Time re-

- solved reflectance and transmittance for the non-invasive measurement of tissue optical properties," *Appl. Opt.* **28**, 2331–2336 (1989).
37. C. A. Haniff, "Least-squares Fourier phase estimation from the modulo 2π bispectrum phase," *J. Opt. Soc. Am. A* **8**, 134–140 (1991).
 38. C. L. Matson, "Weighted-least-squares phase reconstruction from the bispectrum," *J. Opt. Soc. Am. A* **8**, 1905–1913 (1991).
 39. J. C. Marron, P. P. Sanchez, and R. C. Sullivan, "Unwrapping algorithm for least-squares phase recovery from the modulo 2π bispectrum phase," *J. Opt. Soc. Am. A* **7**, 14–20 (1990).
 40. A. A. Scribot, "First-order probability density functions of speckle measured with a finite aperture," *Opt. Commun.* **11**, 238–241 (1974).
 41. B. C. Park and M. S. Chung, "First-order probability density function of the integrated speckle," *Opt. Commun.* **83**, 5–9 (1991).
 42. N. George, "Speckle at various planes in an optical system," *Opt. Eng.* **25**, 754–764 (1986).
 43. H. Fujii and T. Asakura, "Effect of the point spread function on the average contrast of image speckle patterns," *Opt. Commun.* **21**, 80–84 (1977).
 44. A. Papoulis, *Probability, Random Variables, and Stochastic Processes*, 3rd ed. (McGraw-Hill, Boston, Mass., 1991).
 45. M. A. Berger, *An Introduction to Probability and Stochastic Processes* (Springer-Verlag, New York, 1993).
 46. P. Billingsley, *Probability and Measure*, 3rd ed. (Wiley, New York, 1995).
 47. D. Middleton, *An Introduction to Statistical Communication Theory* (McGraw-Hill, New York, 1960).
 48. R. A. Wooding, "The multivariate distribution of complex normal variables," *Biometrika* **43**, 212–215 (1956).
 49. T. L. Grettenberg, "A representation theorem for complex normal processes," *IEEE Trans. Inf. Theory* **IT-11**, 305–306 (1965).